

Combined inelastic neutron scattering and solid-state density functional theory study of dynamics of hydrogen atoms in muscovite $2M_1$

L'UBOMÍR SMRČOK,^{1,*} MILAN RIEDER,² ALEXANDER I. KOLESNIKOV,³ AND GARRETT E. GRANROTH³

¹Institute of Inorganic Chemistry, Slovak Academy of Sciences, Dúbravská cesta 9, SK-845 36 Bratislava, Slovak Republic

²Czech Geological Survey, Geologická 6, 152 00 Praha 5, Czech Republic and CPIT, VŠB-TU Ostrava, 17. listopadu 15, 708 33 Ostrava-Poruba, Czech Republic

³Neutron Scattering Sciences Division, Oak Ridge National Laboratory, Oak Ridge, Tennessee 37831, U.S.A.

ABSTRACT

Inelastic neutron scattering (INS) was used to study dynamics of the hydrogen atoms in natural $2M_1$ muscovite in the 150–1200 cm^{-1} energy range. The resultant INS spectra are interpreted by means of solid-state density functional theory calculations covering both normal mode analysis and molecular dynamics. While signatures of the Al-O-H bending modes were found over the whole energy transfer range, the dominant contributions were observed between 800–1000 cm^{-1} . The modes assigned to the in-plane movements of the respective hydrogen atoms are well defined and always appear at high energies. In contrast, the modes corresponding to the out-of-plane movements are spread over large energy transfer ranges, extending down to the region of external (lattice) modes. The positions of the high-energy modes contributing to the INS band at $\sim 907 \text{ cm}^{-1}$ depend on the distance of respective hydrogen atoms to the nearest oxygen atom of the basal net and its polarity.

Keywords: Inelastic neutron scattering, muscovite, DFT, vibrational spectra, molecular dynamics

INTRODUCTION

To elucidate proton dynamics in the 2:1 sheet silicates, we have carried out a combined inelastic neutron scattering and solid-state computational study of the dynamics of the hydrogen atoms in muscovite, a dioctahedral 2:1 mica. Protons in micas occupy unique positions, because in the structures of these minerals there are no hydrogen bonds of appreciable strengths, which could significantly confine proton motions. The character of their movements manifested by the corresponding vibrational modes thus reflects, in addition to the bond bending modes, the dynamics of the deformational changes of the polyhedra forming the 2:1 layer as well as the mutual movements of entire 2:1 mica layers. Furthermore, the movements of protons can be influenced by inhomogeneities in their surroundings originating mainly from the chemical variability in the cation positions of the constituting polyhedra. Therefore, the protons can help reveal some fine structural details.

The comprehensive review of Beran (2002) shows that considerable effort has been invested in studying the proton dynamics in micas by conventional IR or Raman spectroscopy, especially within the energy transfer region $\sim 3000\text{--}3600 \text{ cm}^{-1}$. This region is the home to the OH stretching modes, which appear uncontaminated by any other vibrational modes. Their unique positions facilitate their measurement, making them a subject of numerous studies. On the other hand, the region of X-O-H (X being Al, Mg, Fe, etc.) deformation modes ($<1500 \text{ cm}^{-1}$) is only rarely examined in the context of proton dynam-

ics because the contributions of the proton containing groups to the optical vibrational spectra are masked by much stronger contributions arising from the motions of heavier atoms (Farmer and Russell 1964).

The use of INS to study proton dynamics has several advantages over the well-established IR or Raman spectroscopy. In particular, hydrogen has by far the largest incoherent neutron scattering cross-section of all elements and thus the signatures of hydrogen motions are the most prominent features of any INS measurement. Furthermore, for INS there are no selection rules that cause several modes to be absent (Dove 2002; Chaplot et al. 2002; Mitchell et al. 2005). Finally, the measured INS intensities are directly proportional to the mean square displacements of the hydrogen atoms in the corresponding modes. Therefore, the standard methods of normal modes analysis (NMA) or Fourier transform power spectra of individual velocity autocorrelation functions obtained by molecular dynamics simulations can be used to model the measurements. The power of the INS as a probe of hydrogen atoms dynamics can be further enhanced by combining it with the predictive capabilities of theoretical methods, in particular of modern solid-state density functional theory (DFT) calculations.

We have recently applied this approach successfully in the INS/DFT studies of hydrogen atoms dynamics in kaolinite-DMSO intercalate and in a highly ordered kaolinite (Smrčok et al. 2010a, 2010b), where not only detailed assignments of the individual vibrational modes were presented, but where also the influence of O-H...O hydrogen bonds on the interlayer proton dynamics was documented. An interesting result of both studies was that the modes generated by the protons positioned inside

* E-mail: uachsmrk@savba.sk

the kaolinite 1:1 layer (intralayer) mirror various deformations of the polyhedra and also of the entire layer. However, due to heavy overlaps of the individual contributions in the energy region below ~ 700 cm^{-1} , full separation of the contributions of the hydrogen atoms involved in the interlayer hydrogen bonds from the contributions generated by the intralayer protons is not possible.

In contrast to 1:1 sheet silicates, all protons in micas are intralayer and provide thus a unique chance for a thorough analysis of the dynamics of the silicate 2:1 layer. The aim of this study is the basic interpretation of the vibrational INS spectrum of a dioctahedral $2M_1$ polytype of muscovite within the low and middle energy transfer range. The main purpose of our investigation is to describe the dynamics of the hydrogen atoms in the muscovite structure and to relate the information obtained by vibrational spectroscopy to the crystal structure. The study is a part of our investigation of proton dynamics in sheet silicates by INS vibrational spectroscopy and the theoretical calculations in the solid state (Scholtzová and Smrček 2009; Smrček et al. 2010a, 2010b).

The main computational apparatus employed is the solid-state theoretical calculation at DFT level of theory inasmuch as it offers both local and global structural information. The tools used in the analysis, i.e., partial vibrational densities of states (PVDOS) of the hydrogen atoms, were obtained both within the harmonic approximation (“normal mode analysis,” NMA) as well as by molecular dynamics calculations that go beyond the limits of harmonic approximation. Although the intensities of such calculated spectra are not entirely equivalent to those obtained by INS, they provide unique insight into the nature of individual vibrational processes.

EXPERIMENTAL AND CALCULATION

Our study required a sample that crystallized at a relatively low temperature to minimize the solid solutions and thus we opted for a muscovite from a pegmatite. Such a mica should exhibit a very limited solid solution toward paragonite or the celadonites. The muscovite used comes from a pegmatite on Fučná hill near Otov, Czech Republic. It was collected in 1961, when the pegmatite was mined for feldspar. (For a list of minerals reported from the locality see Kratochvíl 1962, p. 70–72.) Such muscovite occurs in large crystals that are free from heterogeneous impurities. For the studied sample, one such book of muscovite was cut with scissors and then milled, under ethyl alcohol, in a Fritsch agate ball mill at maximum speed for 10 min. Because there is no published chemical analysis of muscovite from Otov, elemental analysis was carried out by energy dispersive X-ray analysis (EDX) using a Carl Zeiss EVO40HV scanning electron microscope (SEM), with an accelerating voltage of 20 kV. Depending on the valence of iron, two slightly different chemical formulas can be calculated (Table 1). In terms of their *mgli* and *feal* coordinates (Tischendorf et al. 2004), both plot in the field of most frequent muscovite compositions (Tischendorf et al. 2007, Fig. 1 therein) and close to the muscovite end-member formula. Thus, this muscovite sample is sufficiently pure for this study.

The lattice parameters of the muscovite were refined by the LeBail technique as implemented in the FullProf code (Rodríguez-Carvajal 1993) using a diffraction pattern taken with a Stoe Stadi P transmission diffractometer with strictly monochromatic $\text{CoK}\alpha_1$ radiation (Fig. 1). The starting values of the lattice parameters were taken from Rothbauer (1971) and, since the refined and the published values are consistent, the computational model was based on the published values.

The INS spectra were collected with the direct geometry time-of-flight spectrometer SEQUOIA (Granroth et al. 2006, 2010) installed at the Spallation Neutron Source, Oak Ridge (Tennessee). The SEQUOIA spectrometer can finely resolve energy transfers (as fine as 1–1.5% E_i) for incident neutron energies (E_i) between 80 and 16000 cm^{-1} (10 meV and 2 eV). The source power was about 400 kW during the experiments, which provided a neutron flux on the sample of ~ 7

TABLE 1. Energy dispersive analysis of muscovite from Otov-Fučná and its crystallochemical formula, recalculated to 22(+) cation charges

	Analysis (atoms)	Formula 1	Formula 2
K	5.0(2)	0.85	0.86
Na	0.52(8)	0.09	0.09
Σ interlayer atoms		0.94	0.95
Mg	0.31(7)	0.05	0.05
Fe_{tot}	0.89(4)		
Fe^{3+}		0.15	
Fe^{2+}			0.15
Al_{tot}	16.8(8)		
Al		1.85	1.89
Σ octahedral atoms		2.05	2.09
Si	17.4(8)	2.97	2.99
Al		1.03	1.01
Σ tetrahedral atoms		4.00	4.00
<i>mgli</i> (Mg-Li)		0.05	0.05
<i>feal</i> ($\text{Fe}_{\text{tot}}^{\text{VI}}/\text{Al}$)		-1.7	-1.74

Note: Alternatives are given corresponding to all Fe as Fe^{3+} (Formula 1) or as Fe^{2+} (Formula 2).

$\times 10^4$ n/cm²/s for the $E_i = 100$ meV. A 5.5 m radius cylindrical detection array of 25 mm wide by 10 mm high pixels is located downstream of the sample position. This detector array covers -30° and 60° in the horizontal plane and $\pm 18^\circ$ in the vertical plane. One gram of muscovite powder sample was placed in an aluminum container to cover a beam size of 20 mm (h) by 50 mm (v) and measured at $T = 6$ K with $E_i = 46, 137,$ and 224 meV ($-368, 1096,$ and 1792 cm^{-1}) selected by the Fermi chopper rotating at 540, 600, and 600 Hz, respectively. Several E_i values were chosen to ensure fine resolution over a wide energy range. The background spectra measured from the empty sample container under the same conditions, were subtracted from the sample data. The neutron scattering data were first transformed from time-of-flight and instrument coordinates to the dynamical structure factor $S(Q, E)$ (Marshall and Lovesey 1971). These data were further reduced to the generalized density of phonon states $G(E)$ by using the expression,

$$S(Q, E) = \frac{Q^2 [n(E, T) + 1]}{E} G(E)$$

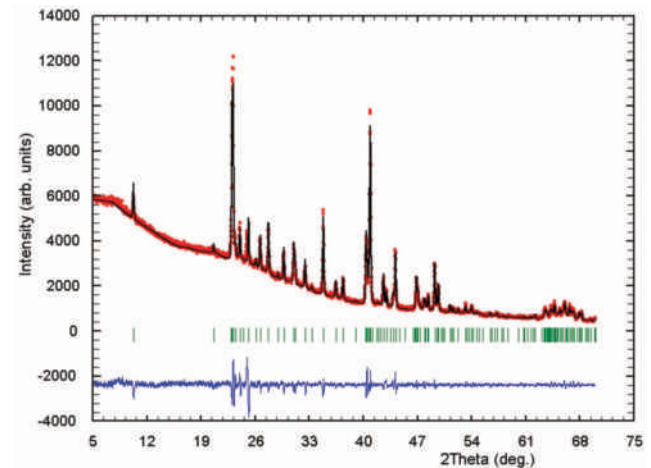


FIGURE 1. LeBail fit to the transmission powder diffraction pattern. $R_{\text{wp}} = 0.19$, $R_{\text{B}} = 0.07$. The experimental pattern is shown by dots, the calculated profile by a solid line overlying them. Small vertical bars indicate the positions of Bragg peaks; the lower curve shows the difference between the observed and calculated intensities. The list of refined values included the lattice parameters, a zero point correction, an overall displacement parameter Q (\AA^2) and the U and W parameters of the FWHM model. Background variation was modeled by a linear approximation between manually selected points.

where $n(E, T)$ is the population Bose factor, Q and E are momentum and energy transfer values, and T is the temperature.

The solid-state DFT calculations were performed using the VASP program (Kresse and Hafner 1993; Kresse and Furthmüller 1996a, 1996b). The initial positions of all atoms were taken from Rothbauer (1971) and expanded to the space group $P1$. In accordance with the estimated chemical composition, four tetrahedral Si atoms were replaced by four non-neighboring Al atoms (Fig. 2). Their placement within the layer was not optimized, as their distribution in the muscovite structure is most probably random (Catti et al. 1994). The electron exchange-correlation interaction was described in the generalized gradient approximation (Perdew and Wang 1992). Plane waves formed the basis set and calculations were performed using the projector-augmented wave method (Blöchl 1994; Kresse and Joubert 1999) and atomic pseudo-potentials (Kresse and Hafner 1994). The energy cutoff controlling the accuracy of the calculation was set to 500 eV; representing an extended basis set and consequently highly accurate calculations. The positions of all atoms were optimized by means of the conjugated gradient method in the four k -points (Teter et al. 1989; Bylander et al. 1990) with the unit-cell parameters fixed. The structure was optimized mainly to rationalize the positions of the atoms in the tetrahedra because the sizes of the Si and Al tetrahedra are sufficiently different to cause local structure deformations (Scholtzová and Smrček 2005). Considering the size of the unit cell, the calculations were restricted to the γ point of the Brillouin zone. The normal modes were calculated in the harmonic approximation with the total energy converged to 10^{-7} eV and with the residual forces on the atoms smaller than 0.005 eV/Å. The Hessian was constructed from the single-point energy calculations of the $6n$ structures generated from the optimized structure by displacing each of the n atoms in the cell in the positive and negative senses along the Cartesian directions x , y , and z (Hafner 2003). Because the measured spectrum starts at ~ 150 cm^{-1} , no dispersion effects were included in the calculations.

Owing to the large computational demands for the molecular dynamics calculations (MD) the energy cutoff was set to 400 eV, the number of k -points to two and the required convergence in total energy to 10^{-4} eV. The finite temperature calculations were performed on a canonical ensemble with a Nosé thermostat procedure (Nosé 1984) at the simulation temperature of 300 K. The Verlet velocity algorithm (Ferrario and Ryckaert 1985) was used over a simulation interval of 65 ps with a 1 fs step size. The results of the MD calculations were interpreted in frequency space by calculating the Fourier transform of the individual velocity autocorrelation functions and presented as power spectra (PS). Partial vibrational densities of states (PVDOS) were calculated using the aClimax code (Ramirez-Cuesta 2004) with arbitrarily chosen peak widths. The basic geometry of the optimized structure was analyzed using the PLATON program (Spek 2002) and the calculated modes were analyzed with the help of the MOLEKEL program (Portmann and Luthi 2000).

RESULTS AND DISCUSSION

Structure optimization

The resulting atomic coordinates, the essential bond distances and angles and the derived geometric characteristics of individual coordinations are given in Tables 2 and 7, and deposit Tables 3–6¹. In the triclinic description, there are eight tetrahedra, all quite regular, with the effective coordination number (ECoN) close to the ideal 4.0 and quadratic elongation close to 1.0. However, the angle variance is diversified, but there appears to be no systematic pattern. The most visible difference is in the cation-ligand bond length, which is clearly shorter in tetrahedra occupied by Si than in those occupied by Al. These bond lengths agree remarkably well with those obtained by adding Shannon and Prewitt's (1969) ionic radii values of Si^{4+} (0.26 Å) or Al^{3+} (0.39 Å) to that of O^{2-} (1.38 Å, all for coordination IV). Naturally, different cation-ligand bond lengths are projected into the O-O bond lengths and, in turn,

into the polyhedral volumes. The four Al-occupied octahedra are practically identical. Specifically, they all display the same, considerable counter-rotation of the top and bottom oxygen triads. Dioctahedral micas are known for their tetrahedral rotation, which negatively correlates with the effective coordination number of the interlayer cation (Weiss et al. 1992, their Fig. 12), and the present data agrees with this observation.

O-H modes by normal mode analysis and molecular dynamics

The shapes of the predicted PVDOS-es (Fig. 3) indicate that the individual experimental INS peaks are not associated with the single energy transfers. The NMA shows that the high energy transfer band (~ 907 cm^{-1}) is the sum of modes (Table 8) reflecting the motion of the hydrogen atoms in the plane, which is approximately parallel to the plane fit to the apical oxygen atoms of the respective $\text{Si}(\text{Al})\text{O}_4$ tetrahedra (in-plane bending modes, ip).

These modes are predicted to be distributed over a wide energy range of ~ 100 cm^{-1} . Note that although the state of all the hydrogen atoms in the structure of mica is formally similar to those of the inner hydroxyl groups in kaolinite, in our computational model they reside, compared to kaolinite, in two different environments (Fig. 4). It is therefore proposed that the mutual shifts of the main peaks of the ip bending modes are caused by a

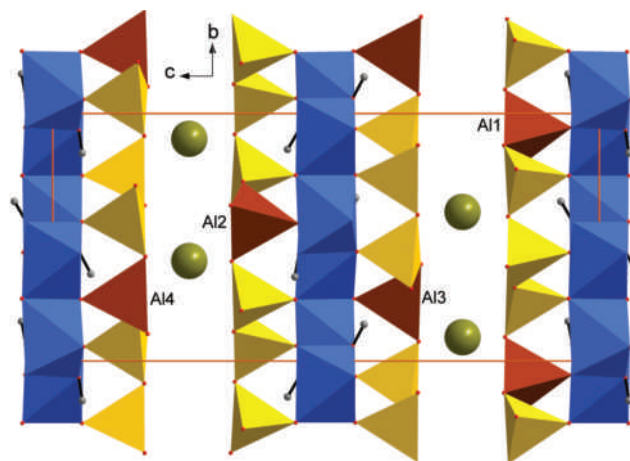


FIGURE 2. Polyhedral presentation of the crystal structure of muscovite projected along the a -axis. Large balls represent interlayer potassium and small balls intralayer hydrogen atoms. The figure was prepared using the program DIAMOND (Brandenburg 2006).

TABLE 2. Crystal data

Formula	$\text{Al}_6\text{H}_4\text{O}_{24}\text{Si}_6$ 2(K)
Formula weight	796.65
Crystal system	Triclinic
Space group	$P1$ (No. 1)
a	5.1918(3)
b	9.0153(5)
c (Å)	20.046(2)
α	90
β	95.74(2)
γ (°)	90
V (Å ³)	933.56
Z	2
D_{calc} (g/cm ³)	2.834
μ (MoK α) (mm)	1.310
$F(000)$	792

¹ Deposit item AM-11-011, Tables 3–6 and data set. Deposit items are available two ways: For a paper copy contact the Business Office of the Mineralogical Society of America (see inside front cover of recent issue) for price information. For an electronic copy visit the MSA web site at <http://www.minsocam.org>, go to the *American Mineralogist* Contents, find the table of contents for the specific volume/issue wanted, and then click on the deposit link there.

TABLE 7. Distortion characteristics of coordination polyhedra in muscovite

Polyhedron	Bond	MEFBL	Mean	ECoN	Polyhedral volume	Quadratic elongation	Angle variance	Counter-rotation	Rotation of tetrahedra
Tet Si2	cation-O	1.638	1.639(12)	3.98	2.24957	1.00357	13.26		
	O-O		2.676(24)						
Tet Si4	cation-O	1.640	1.641(5)	4.00	2.26369	1.00062	2.38		
	O-O		2.679(10)						
Tet Si6	cation-O	1.642	1.644(15)	3.96	2.27685	1.00166	6.29		
	O-O		2.684(13)						
Tet Si7	cation-O	1.639	1.642(15)	3.96	2.26581	1.00183	5.89		
	O-O		2.681(18)						
Tet Si8	cation-O	1.640	1.640(9)	3.99	2.25910	1.00193	7.02		
	O-O		2.678(18)						
Tet Si10	cation-O	1.637	1.639(13)	3.97	2.25332	1.00249	10.16		
	O-O		2.675(15)						
Tet Al1	cation-O	1.762	1.762(6)	3.99	2.78495	1.00535	20.35		
	O-O		2.876(32)						
Tet Al4	cation-O	1.757	1.757(8)	3.99	2.78115	1.00105	3.87		
	O-O		2.869(14)						
Oct Al5	cation-O	1.924	1.929(18)	5.90	9.30191	1.01973	68.8		
	O-O unshared		2.823(23)					15.1(2.5)	
	O-O shared longer		2.866(72)						
	O-O shared shorter		2.413(13)						
Oct Al7	cation-O	1.921	1.928(19)	5.88	9.28962	1.01891	65.6		
	O-O unshared		2.811(28)					15.4(3.0)	
	O-O shared longer		2.876(17)						
	O-O shared shorter		2.415(14)						
Oct Al9	cation-O	1.921	1.924(13)	5.95	9.24966	1.01754	62.9		
	O-O unshared		2.802(21)					15.5(2.0)	
	O-O shared longer		2.874(35)						
	O-O shared shorter		2.416(38)						
Oct Al11	cation-O	1.919	1.926(19)	5.88	9.27775	1.01817	63.4		
	O-O unshared		2.813(19)					15.0(1.1)	
	O-O shared longer		2.861(20)						
	O-O shared shorter		2.414(38)						
Int K1	cation-O	2.791	3.14(12)	6.83					16.3(6)
Int K3	cation-O	2.770	3.11(12)	6.77					16.4(5)

Notes: "Tet" = tetrahedron, "Oct" = octahedron, "Int" = interlayer. Lengths are in angstroms, volumes in Å³. Errors (in parentheses) are given as one e.s.d. The quantities given in the table were obtained using the programs DIAMOND (Brandenburg and Putz 1997–2007), MOLDRAW (Ugliengo et al. 1988), and VOLCAL (Finger and Ohashi 1979). The MEFBL is the bond length weighted as in the calculation of MEFIR (Hoppe 1979). The formulas for counter-rotation of the top and bottom oxygen triads in the octahedra and for the tetrahedral rotation angle were taken from Weiss et al. (1985, 1992).

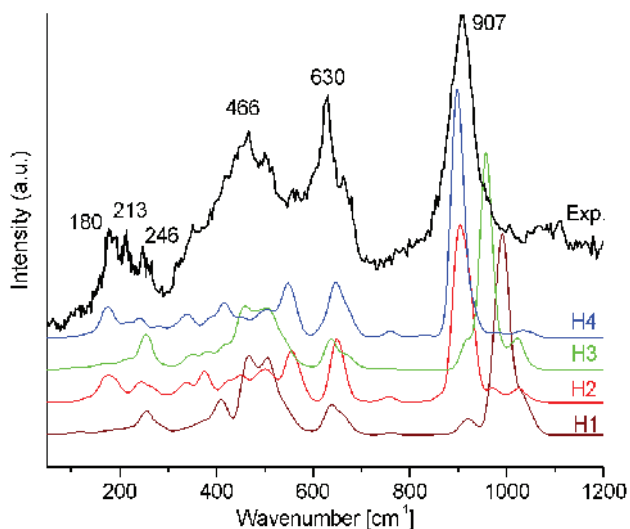


FIGURE 3. Calculated partial vibrational densities of states (PVDOS) for the respective hydrogen atoms compared to the measured INS spectrum transformed to $G(E)$ on the top. Because the predicted PVDOS for H5, H6, H7, and H8 are indistinguishable from those of H4, H3, H2, and H1, respectively, they are not shown. Positions of the peaks in the INS spectrum are estimated as the positions of local maxima. Each calculated spectrum is normalized to the highest intensity value and offset by a constant for the sake of clarity.

synergic effect of three factors: (1) the distance of each hydrogen atom to the nearest bridging oxygen atom of the basal net; (2) O-H...O (basal) contact angle and (3) the polarity of the basal oxygen atom influencing the strength of the H...O interaction. This hypothesis is supported by the predicted positions of the main peaks of the *ip* modes, which are inversely proportional to the individual H...O separations and the O-H...O bond angles. As to the polarity of the bridging oxygen atoms, the oxygen atom linking Si and Al atoms can be shown to be more negative than the one linking two Si atoms. For example, from the molecular DFT (BP/SVP) calculations of the $[\text{Si}_5\text{AlO}_{18}\text{H}_{12}]^{-1}$ cluster representing a ditricon of a tetrahedral sheet it follows that in the latter case the calculated Mulliken charge on the oxygen atom is $-0.456 |e|$, while in the Al-O-Si case it is significantly larger, $-0.548 |e|$ (Tunega 2009). Interestingly, Liang and Hawthorne (1998) suggested the existence of two (or even more) distinct OH groups in the structure of muscovite by considering the shape of the OH stretching band obtained by photoacoustic FTIR spectroscopy. However, their attempts to support this hypothesis by means of a structure refinement with a split hydrogen atom position added to Rothbauer's model led to inconclusive results. Although our computational model provides more insight into the hydrogen motions, it is based on several approximations that limit the degree of quantitative agreement with the experiment. Nevertheless, the overall good agreement between the calculated

TABLE 8. Predicted vibrational modes arranged in order of descending energy (cm^{-1})

Si-O s: 1056, 1055, 1054, 1040, 1028, 1027, 1023, 1017, 1015, 1013
Si-O s, Al-O-H b: 1004, 1003, 997, 995, 992, 985, 982, 975, 974, 970, 967, 957, 956, 951, 935, 927, 926, 919, 918, 917, 916, 912, 908, 900, 899, 898, 894, 890, 864
Al(T-O): 834, 824, 799
O-Si-O b: 763, 761, 756
O-Si-O b, Al(T)-O s: 737, 735, 729, 728
Al(T)-O s, T-O-T b: 713, 712, 701
T-O-T b, T-O-Al(Oc) b: 699, 686
T-O-T b, T-O-Al(Oc) b, op Al-O-H b: 684, 682, 681, 669, 666, 664, 657, 656, 645, 639, 638, 635, 631, 621, 617, 604, 601, 592, 591
T-O-T b, T-O-Al(Oc) b, Al(Oc)-O s, op Al-O-H b: 577, 575, 568, 562, 556, 554
2:1 layer deformation, op Al-O-H b: 549, 545, 539, 525, 519, 518, 513, 511, 506, 505, 501, 499, 491, 487, 483, 479, 469, 468, 463, 462, 458, 456, 449, 437, 436, 426, 425, 421, 419, 415, 413, 411, 410, 405, 404, 401, 395, 394, 386, 379, 377, 375, 373, 364, 363, 356, 355, 355, 353, 343, 342, 340, 335, 334, 327
Octahedra wobbling inducing deformations of 2:1 layer ("layer breathing"): 326, 324, 317, 313, 312, 309, 306, 303, 302, 299, 298, 294, 292, 287, 285, 283, 280, 275, 274, 270, 268, 265, 256, 254, 252, 250, 247, 245, 241, 239, 232, 228, 227, 223, 217, 216, 213, 210, 192, 191, 187, 186, 180, 176, 174, 172, 171, 169
Rattling of the 2:1 layer, O-K-O deformations: 163, 158, 157, 152, 151, 149, 147, 144, 140, 137, 134, 132, 130, 126, 122, 119, 118, 114, 110, 107, 105, 101
Mutual shifts of 2:1 layers: 83, 82, 66, 45, 38

Notes: s,b = stretching, bending mode; ip, op = in plane, out of plane bending mode; Al(T), Al(Oc) = tetrahedral, octahedral aluminum, T = a tetrahedral cation.

and observed spectra is evident and allowed unambiguous assignment of the modes.

The region around 800 cm^{-1} , represented by a valley in the experimental spectrum, is allocated to the O-Si-O bending modes (Table 8). Because the scattered intensity drops to the

background level, the impact of the O-Si-O deformations on the movements of the hydrogen atoms can be neglected. The sharp band with the dominant peak at $\sim 630 \text{ cm}^{-1}$ is formed by the contributions from all hydrogen atoms, although the shapes of individual contributions are somewhat different (Fig. 3). All these modes correspond to the hydrogen atoms moving nearly perpendicular to the reference plane (out-of-plane bending, *op*) defined by the apical oxygen atoms. Similar energies of all these modes suggest that the corresponding movements are, for the most part, independent of the different environment surrounding each hydrogen atom. Beside the main contributions arising from the pure Al-O-H bending modes, manifested in the central sharp peak predicted at $\sim 645 \text{ cm}^{-1}$, the spectrum also reflects some secondary hydrogen atom motions induced by deformations in individual polyhedra of the 2:1 layer (Table 8). The amplitudes of these movements are, however, small compared with the amplitudes of the pure Al-O-H bending modes, and the vibrational energies of the corresponding contributions forming the broader base of the band are comparable.

The region of the well-defined peaks in the calculated PVDOS ends at $\sim 600 \text{ cm}^{-1}$. Below this limit, the PVDOS can be divided into two groups according to their shapes; the contributions of the H1 and H3 atoms being in the first and the H2 and H4 atoms in the second. The contributions from the interaction of the first group with the more negative oxygen atoms are concentrated mostly in the dominating multiplets centered around $\sim 500 \text{ cm}^{-1}$ and end with the pronounced bands at $\sim 255 \text{ cm}^{-1}$. The profiles of the H1 and H3 multiplets thus control the shape of the band

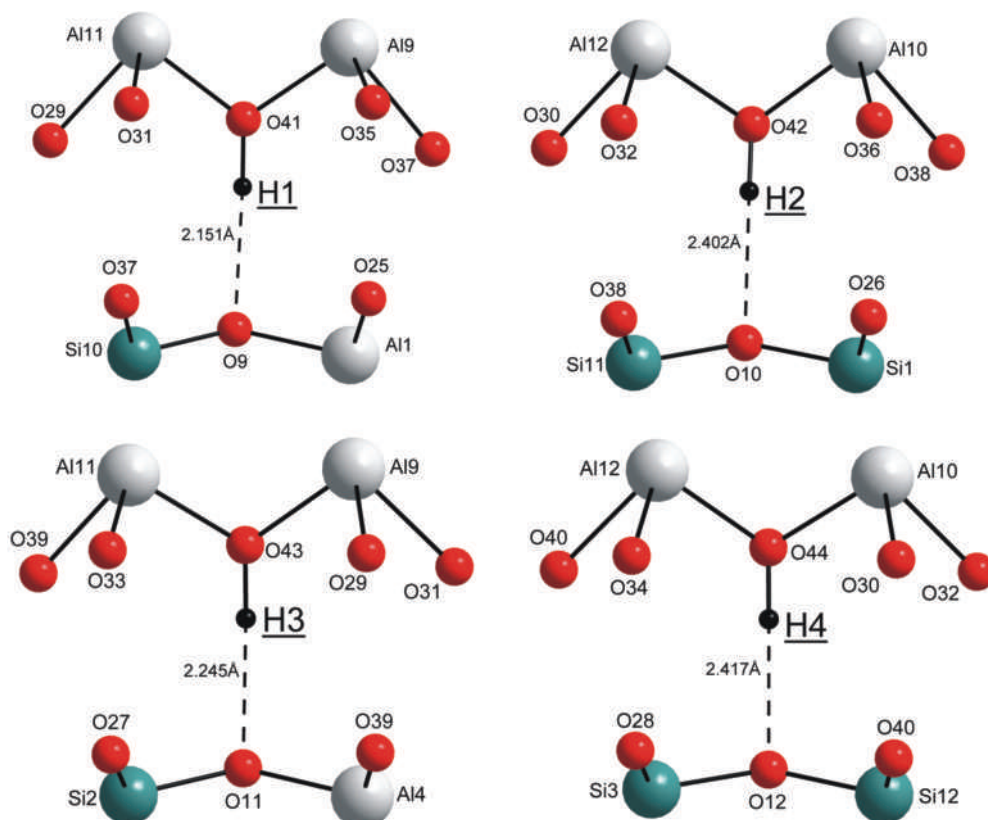


FIGURE 4. Fragments of the structure showing non-bonding H...O (basal) contacts for H1–H4 atoms. The O-H...O contact angles ($^{\circ}$) are 157° (H1), 134° (H2), 155° (H3), and 135° (H4), respectively.

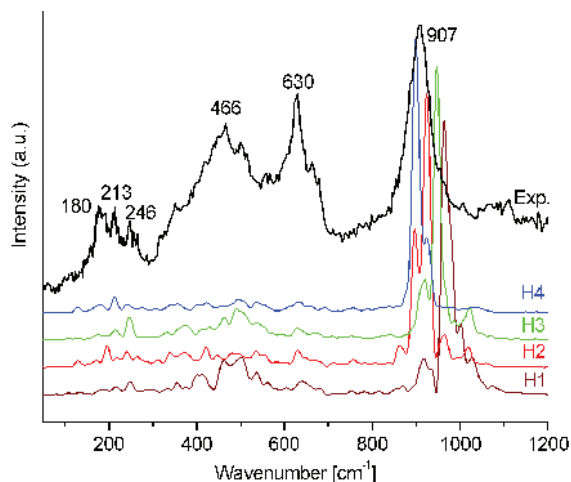


FIGURE 5. Measured INS spectrum transformed to $G(E)$ (top) and the power spectra calculated for the respective hydrogen atoms. Positions of the peaks in the INS spectrum are estimated as the positions of local maxima. Each calculated spectrum is normalized to the highest intensity value and offset by a constant for the sake of clarity.

centered in the INS spectrum at ~ 466 cm^{-1} . This picture is in contrast with the dispersed excitations obtained for the H2 and H4 group, which face less negatively charged oxygen atoms of the tetrahedral net. These lines end with peaks situated at lower energies than those generated by the H1/H3 couple, i.e., near 175 cm^{-1} . The valley between the bands, bounded by the maxima at 630 and 466 cm^{-1} , is filled by the *op* modes involving just the atoms of the second group. A closer examination of the calculated modes shows that within the region between 550 and 320 cm^{-1} the movements of hydrogen atoms are best described as a mixture of several autonomous *op* Al-O-H bending modes modulated by various deformations of the 2:1 layer. The lowest energy band, spanning (300 to 180 cm^{-1}) reveals octahedral oscillations (“wobbling”) inducing thus deformations of the whole 2:1 layer (down to 300 cm^{-1}) and the 2:1 “layer breathing” modes (down to ~ 170 cm^{-1}). Note that the modes in the latter region could partially overlap with the lattice modes, which are not accurately simulated by the calculation.

The power spectra (PS) of the individual hydrogen atoms H1–H4 along with the experimental INS spectrum are shown in Figure 5. The positions of the maxima of the four multiplets corresponding to the 907 cm^{-1} peak in the INS spectrum correlate reasonably well with the positions of the *ip* modes predicted by the NMA. The most evident disagreement between the results of the PS and NMA is the shape of the individual contributing bands, as those calculated by PS are in general more structured. The main peaks attributed to the H2 and H4 atoms are doublets with pronounced major and minor components, while the peaks for the H1 and H3 atoms have only small side bands. More importantly, there are noticeable differences in the central peak positions of H2 and H4, which are practically indistinguishable in the harmonic approximation. In contrast, the discrepancies in the shapes of the modes predicted for the H1 and H3 atoms by both methods are small. The PS region below 700 cm^{-1} is not interpreted because the contributions of individual hydrogen atoms have too few prominent features.

Comparison with previously published data on X-O-H deformation modes

In the IR study of vibrations of the OH ions in muscovite Vedder and McDonald (1963) identified two low-energy absorption bands at 925 and 405 cm^{-1} . Using our terminology, the former can be attributed to the *ip* and the latter to the *op* modes.² Later, Vedder (1964, Table 3 therein) identified in the IR spectrum of a Brazilian muscovite seven “OH libration modes” in the range 928–351 cm^{-1} . A comparison with the INS spectrum shows that the modes at 928 and 630 cm^{-1} can be associated with well defined INS bands peaking at 907 and 630 cm^{-1} , and the next two modes, 405 and 351 cm^{-1} , can form a part of the composite INS band with a maximum at 466 cm^{-1} . However, the assignment of the three modes between 805–691 cm^{-1} is inconsistent with the intensity valley in the INS spectrum.

Loh (1973) assigned the bands recognized at ~ 190 , 240, and 265 cm^{-1} to unspecified “internal vibrations of the isosceles triangle O-H-O,” where the oxygen atoms are the non-bridged atoms from the neighboring SiO_4 tetrahedra and H is the hydrogen of the OH ion tilted toward the octahedral vacancy. Although the energies of these modes are close to the energies of one sharp and one composite band appearing in the INS spectrum at 213 and 246 cm^{-1} , the uncertainty in their definition prevents a direct reconciliation with the calculated ones. On the other hand, it is fair to assume that the band at 196 cm^{-1} assigned by Loh to the “distortion of M-O_6 ” octahedron is reflected in the INS spectrum. Similar octahedral deformations and “OH translation” modes have also been identified in the low-energy transfer region in a Raman study of muscovite $2M_1$ (McKeown et al. 1999).

Investigation of lattice dynamics in muscovite by INS (Wada and Kamitakahara 1991) focused only on the energy transfer range below 45 cm^{-1} , which is not covered by our experiment. Those data were later used by Gupta et al. (1994) as a benchmark for phonon dispersion calculations based on empirical potentials. Their predicted highest energy band is consistent with the low-energy end of the cluster centered at ~ 200 cm^{-1} in the INS spectrum and probably corresponds to octahedral deformation modes (Table 8).

The existence of an OH band at 1165 cm^{-1} attributed to “in-plane librational T-OH mode” in Ge-muscovite (Ackermann et al. 1993) was explained by bonding of “apical” OH groups directly to tetrahedral atoms. The present study provides no further input on this point, and this proposal should be confirmed either by diffraction study or by solid-state theoretical calculations.

Vibrational energies of the bridging (M-OH-M') hydroxyl groups were theoretically predicted at the Hartree-Fock/6-31+G* level of theory (Sainz-Diaz et al. 2000). The computational model derived from the pyrophyllite structure was a molecular cluster built around two central cations. Despite the simplicity of the model, the vibrational energy values (M = M' = Al, 914 cm^{-1} for *ip* and 449 cm^{-1} for *op* mode) agree well with the bands positions in our INS spectrum. The vibrational energy for the *ip* and *op* modes (874+866/452 cm^{-1}) as obtained for 2:1 mineral pyrophyllite by the solid-state DFT calculation (Botella et al.

² The authors stated that the priority in assigning the former to OH bending vibrations belongs to Beutelspacher (1956).

2004) quantitatively agree with the positions of similar modes in the presented INS spectrum of muscovite.

ACKNOWLEDGMENTS

The work at Spallation Neutron Source was supported by Oak Ridge National Laboratory, managed by UT-Battelle, LLC, for the U.S. Department of Energy under Contract No. DE-AC05-00OR22725. We are thankful to T.E. Sherline for assistance with the INS experiments conducted at the SNS. L.S. acknowledges the financial support of the Slovak Grant Agency VEGA under the contract 2/0150/09, M.R. a partial support by grant no. 205/08/0122 from the Czech Grant Agency. This work has also benefited from the Centers of Excellence program of the Slovak Academy of Sciences (COMCHEM, Contract no. II/1/2007).

REFERENCES CITED

- Ackermann, L., Langer, K., and Rieder, M. (1993) Germanium muscovites with excess hydroxyl water, $KAl_2[Ge_{3-x}Al_{1+x}O_{10-x}(OH)_x(OH)_2]$ and the question of excess OH in natural muscovites. *European Journal of Mineralogy*, 5, 19–29.
- Beutelspacher, H. (1956) VIth International Congress of Soil Science, 329–355.
- Blöchl, P.E. (1994) Projector augmented-wave method. *Physical Review B*, 50, 17953–17979.
- Beran, A. (2002) Infrared spectroscopy of micas. In A. Mottana, F.P. Sassi, J.B. Thompson Jr., and S. Guggenheim, Eds., *Micas: Crystal chemistry and Metamorphic Petrology*, vol. 46, p. 351–369. *Reviews in Mineralogy and Geochemistry*, Mineralogical Society of America, Chantilly, Virginia.
- Botella, V., Timon, V., Escamilla-Roa, E., Hernández-Laguna, A., and Sainz-Diaz, C.I. (2004) Hydrogen bonding and vibrational properties of hydroxy groups in the crystal lattice of dioctahedral clay minerals by means of first principles calculations. *Physics and Chemistry of Minerals*, 31, 475–486.
- Bylander, D.M., Kleinman, L., and Lee, S. (1990) Self-consistent calculations of the energy bands and bonding properties of B-12(C-3). *Physical Review B*, 42, 1394–1403.
- Brandenburg, K. (2006) *Diamond. Version 3.1e*. Crystal Impact GbR, Bonn, Germany.
- Catti, M., Ferraris, G., Hull, S., and Pavese, A. (1994) Powder neutron diffraction study of $2M_1$ muscovite at room pressure and at 2 GPa. *European Journal of Mineralogy*, 6, 171–178.
- Chaplot, S.L., Choudhury, N., Ghose, S., Rao, M.N., Mittal, R., and Goel, P. (2002) Inelastic neutron scattering and lattice dynamics of minerals. *European Journal of Mineralogy*, 14, 291–329.
- Dove, M.T. (2002) An introduction to the use of neutron scattering methods in mineral sciences. *European Journal of Mineralogy*, 14, 202–224.
- Farmer, V.C. and Russell, J.D. (1964) The infra-red spectra of layer silicates. *Spectrochimica Acta*, 20, 1149–1173.
- Ferrario, M. and Ryckaert, J.P. (1985) Constant pressure-constant temperature molecular dynamics for rigid and partially rigid molecular systems. *Molecular Physics*, 54, 587–603.
- Finger L.W. and Ohashi Y. (1979) VOLCAL, Program to calculate polyhedral volumes and distortion parameters with errors.
- Granroth, G.E., Vandergriff, D.H., and Nagler, S.E. (2006) SEQUOIA: A fine resolution chopper spectrometer at the SNS. *Physica B*, 385–386, 1104–1106.
- Granroth, G.E., Kolesnikov, A.I., Sherline, T.E., Clancy, J.P., Ross, K.A., Ruff, J.P.C., Gaulin, B.D., and Nagler, S.E. (2010) SEQUOIA: A Newly Operating Chopper Spectrometer at the SNS. *Journal of Physics: Conference series*, in press.
- Gupta, H.C., Sinha, M.M., Rawat, C.C.S., and Tripathi, B.B. (1994) Lattice dynamics of muscovite layered silicates. *Physica status solidi (b)*, 185, 117–121.
- Hafner, J. (2003) Vibrational spectroscopy using ab initio density-functional techniques. *Journal of Molecular Structure*, 651–653, 3–17.
- Hoppe, R. (1979) Effective coordination numbers (ECoN) and mean fictive ionic radii (MEFIR). *Zeitschrift für Kristallographie*, 150, 23–52.
- Kratochvíl, J. (1962) *Topografická mineralogie Čech V*, 491 p. Publishing House of the Czechoslovak Academy of Sciences, Prague (in Czech).
- Kresse, G. and Furthmüller, J. (1996a) Efficient iterative scheme for ab initio total energy calculations using a plane-wave basis set. *Physical Review B*, 54, 11169–11186.
- (1996b) Efficiency of ab-initio total energy calculations for metals and semiconductors using a plane-wave basis set. *Computational Materials Science*, 6, 15–50.
- Kresse, G. and Hafner, J. (1993) Ab initio molecular dynamics for open-shell transition metals. *Physical Review B*, 48, 13115–13118.
- (1994) Norm-conserving and ultrasoft pseudopotentials for first-row and transition elements. *Journal of Physics: Condensed Matter*, 6, 8245–8527.
- Kresse, G. and Joubert, J. (1999) From ultrasoft potentials to the projector augmented wave method. *Physical Review B*, 59, 1758–1775.
- Liang, J.-J. and Hawthorne, F. (1998) Triclinic muscovite: X-ray diffraction, neutron diffraction and photo-acoustic FTIR spectroscopy. *The Canadian Mineralogist*, 36, 1017–1027.
- Loh, E. (1973) Optical vibrations in sheet silicates. *Journal of Physics C: Solid State Physics*, 6, 1091–1104.
- Marshall, W. and Lovesey, S.W. (1971) *Theory of thermal neutron scattering*. Clarendon Press, Oxford.
- McKeown, D.A., Bell, M.I., and Etz, E.S. (1999) Vibrational analysis of the dioctahedral mica: $2M_1$ muscovite. *American Mineralogist*, 84, 1041–1048.
- Mitchell, P.C.H., Parker, S.F., Ramirez-Cuesta, A.J., and Tomkinson, J. (2005) *Vibrational Spectroscopy with Neutrons*, World Scientific, Singapore.
- Nosé, S.J. (1984) A unified formulation of the constant temperature molecular dynamics methods. *Journal of Chemical Physics*, 81, 511–519.
- Perdew, J.P. and Wang, Y. (1992) Accurate and simple analytic representation of the electron-gas correlation energy. *Physical Review B*, 45, 13244–13249.
- Portmann, S. and Luthi, H.P. (2000) MOLEKEL: an interactive molecular graphics tool. *Chimia*, 54, 766–769.
- Ramirez-Cuesta, A.J. (2004) aCLIMAX 4.0.1, The new version of the software for analyzing and interpreting INS spectra. *Computer Physics Communications*, 157, 226–238.
- Rodriguez-Carvajal, J. (1993) Recent Advances in Magnetic Structure Determination by Neutron Powder Diffraction. *Physica B*, 192, 55–69.
- Rothbauer, R. (1971) Untersuchung eines $2M_1$ -Muskovits mit Neutronenstrahlen. *Neues Jahrbuch für Mineralogie, Monatshefte*, 143–154.
- Sainz-Diaz, C.I., Timon, V., Botella, V., and Hernández-Laguna, A. (2000) Isomorphous substitution effect on the vibrational frequencies of hydroxyl group in molecular clusters models of the clay octahedral sheet. *American Mineralogist*, 85, 1038–1045.
- Scholtzová, E. and Smrčok, L. (2005) On local structural changes in lizardite-1T: $\{Si^{4+}/Al^{3+}\}$, $\{Mg^{2+}/Fe^{3+}\}$, $[Mg^{2+}/Al^{3+}]$, $[Mg^{2+}/Fe^{3+}]$ substitutions. *Physics and Chemistry of Minerals*, 32, 362–373.
- Shannon, R.D. and Prewitt, C.T. (1969) Effective ionic radii in oxides and fluorides. *Acta Crystallographica B*, 25, 925–946.
- Scholtzová, E. and Smrčok, L. (2009) Hydrogen bonding and vibrational spectra in kaolinite-dimethylsulfoxide and dimethylselenoxide intercalates—A solid state computational study. *Clays and Clay Minerals*, 57, 54–71.
- Smrčok, L., Tunega, D., Ramirez-Cuesta, A.J., Ivanov, A., and Valúchová, J. (2010a) The combined inelastic neutron scattering (INS) and solid state DFT study of hydrogen atoms dynamics in kaolinite-dimethylsulfoxide intercalate. *Clays and Clay Minerals*, 58, 52–61.
- Smrčok, L., Tunega, D., Ramirez-Cuesta, A.J., and Scholtzová, E. (2010b) The combined inelastic neutron scattering (INS) and solid state DFT study of hydrogen atoms dynamics in highly ordered kaolinite. *Physics and Chemistry of Minerals*, 37, 571–579.
- Spek, A.L. (2002) PLATON. A Multipurpose Crystallographic Tool. Utrecht University, The Netherlands (<http://www.cryst.ch-em.uu.nl/platon>).
- Teter, M.P., Payne, M.C., and Allan, D.C. (1989) Solution of Schrodinger's equations for large systems. *Physical Review B*, 40, 12255–12263.
- Tischendorf, G., Rieder, M., Förster, H.-J., Gottesmann, B., and Guidotti, C.V. (2004) A new graphical presentation and subdivision of potassium micas. *Mineralogical Magazine*, 68, 649–667.
- Tischendorf, G., Förster, H.-J., Gottesmann, B., and Rieder, M. (2007) True and brittle micas: composition and solid-solution series. *Mineralogical Magazine*, 71, 285–320.
- Ugliengo, P., Borzani, G., and Viterbo, D. (1988) MOLDRAW—program for the graphical manipulation of molecules on personal computers. *Journal of Applied Crystallography*, 21, 75.
- Vedder, W. (1964) Correlations between infrared spectrum and chemical composition of mica. *American Mineralogist*, 49, 736–768.
- Vedder, W. and McDonald, R.S. (1963) Vibrations of the OH ions in muscovite. *The Journal of Chemical Physics*, 38, 1583–1590.
- Wada, N. and Kamitakahara, W.A. (1991) Inelastic neutron- and Raman scattering studies of muscovite and vermiculite layered silicates. *Physical Review B*, 43, 2391–2397.
- Weiss, Z., Rieder, M., Chmielová, M., and Krajiček, J. (1985) Geometry of the octahedral coordination in micas: a review of refined structures. *American Mineralogist*, 70, 747–757.
- Weiss, Z., Rieder, M., and Chmielová M. (1992) Deformation of coordination polyhedra and their sheets in phyllosilicates. *European Journal of Mineralogy*, 4, 665–682.